

From emission to absorption: the FAST observation of the OH 18-cm lines from the Comet C/2025 A6

Dongyue Jiang¹, Lei Qian^{2,3,4}, Minglei Guo², Qiaoli Hao², Menglin Huang², Peng Jiang^{2,3}, Hongfei Liu², Chun Sun², Xingyi Wang², Qingliang Yang², Naiping Yu², Lei Zhao², Yutao Zhao², Liyun Zhang^{1,3,5}, Yichi Zhang⁴, Tongjie Zhang^{6,7} and Zhichen Pan^{2,3,4}

¹ Guizhou University, Guiyang 550025, People’s Republic of China

² National Astronomical Observatories, Chinese Academy of Sciences, Beijing 100101, People’s Republic of China; lqian@nao.cas.cn; panzc@nao.cas.cn

³ Guizhou Radio Astronomical Observatory, Guizhou University, Guiyang 550025, People’s Republic of China

⁴ College of Astronomy and Space Sciences, University of Chinese Academy of Sciences, Beijing, 100101, People’s Republic of China

⁵ International Centre of Supernovae, Yunnan Key Laboratory, Kunming 650216, China

⁶ Institute for Frontiers in Astronomy and Astrophysics, Beijing Normal University, Beijing 102206, People’s Republic of China

⁷ School of Physics and Astronomy, Beijing Normal University, Beijing 100875, People’s Republic of China

Received 20xx month day; accepted 20xx month day

Abstract We observed comet C/2025 A6 with the Five-hundred-meter Aperture Spherical radio Telescope (FAST) equipped with the ultra-wideband receiver from 2025 October 23 to November 8, and it was the first detection for this comet with FAST. Through trapezoidal fitting of the OH line profiles, we derived the expansion velocities of the water which showed an increase from $1.5 \pm 0.3 \text{ km s}^{-1}$ at the heliocentric distance of 0.65 AU to $3.0 \pm 0.9 \text{ km s}^{-1}$ at 0.54 AU. Based on these results, we estimated the OH production rates of C/2025 A6 for October 23, October 26, November 4 and November 5 which were $(1.0 \pm 0.1) \times 10^{29}$, $(1.2 \pm 0.1) \times 10^{29}$, $(1.4 \pm 0.3) \times 10^{29}$, and $(1.5 \pm 0.4) \times 10^{29} \text{ s}^{-1}$ respectively. The results show a significant upward trend.

Key words: methods: observational– comets: general– comets: individual: C/2025 A6

1 INTRODUCTION

The comets spend most of their lives in the outer, frozen regions of the solar system. Their chemical compositions preserve crucial information about the primordial environment and the processes that may dominated the Solar System’s formation (Newburn et al. 1991; A’Hearn 2017). When comets approach the Sun, the solar radiation heats their nuclei, causing ices to sublimate, and releasing gases and various molecules into space. Cometary activity can be probed across multiple wavelength regimes with ground-based telescopes, including optical and millimeter/radio observations, among others (e.g., Betzler 2024; Manna et al. 2024; Zhang et al. 2024). As the primary volatile in comets, the production rate and abundance of water provide directly insights into the activity of the

nucleus and its physical properties (Bockelée-Morvan et al. 2004). Under the solar radiation, water molecules undergo photodissociation: $h\nu + \text{H}_2\text{O} \Rightarrow \text{OH} + \text{H}$, producing hydroxyl radicals (OH) via ultraviolet radiation at wavelengths shorter than 186 nm (Crovisier 1989).

Hydroxyl radicals in cometary coma are primarily observed at ultraviolet and radio wavelengths. At radio frequencies, the OH 18-cm lines arise from Λ -doubling and hyperfine transitions within the ground state of the OH radical, distributed near 1612, 1665, 1667, and 1720 MHz (see Table 1). Compared with UV measurements, OH 18-cm lines can be observed from the ground, and less affected by dust extinction. Their narrow profiles provide direct constraints on the gas expansion velocity and kinematic structure of the coma (Bockelée-Morvan et al. 1990). The OH

18-cm line profiles can be used to measure the expansion velocity of water in the cometary coma (Bockelée-Morvan et al. 1990), providing a basis for further studies of the coma’s gas dynamics. Since the first detection the OH 18-cm lines from Comet Kohoutek in 1973 (Biraud et al. 1974), long-term ground-based observations have established extensive datasets of water and OH emissions for a wide variety of comets (e.g., Despois et al. 1981; Crovisier et al. 2002; Wang et al. 2017). These studies have extended observations to comets with different orbital periods and have used variations in molecular production rates to investigate cometary outgassing activity. For comets, either emission or absorption of the OH 18-cm lines could be observed, mainly depending on the comet’s heliocentric radial velocity.

The Comet C/2025 A6 (Lemmon) is a long-period comet. It was discovered by the Mount Lemmon Survey on 2025 January 3 (Fuls et al. 2025), and passed closest to Earth on 2025 October 21, with a geocentric distance of 0.59 AU (from JPL horizons system¹, hereinafter). It subsequently reached perihelion on 2025 November 8, at a heliocentric distance of 0.53 AU. Since the semi-major axis of C/2025 A6 is only about 120 AU, which is considerably smaller than the 10,000 AU threshold typically used to define dynamically new comets (Levison 1996), the comet is likely a returning long-period comet rather than a dynamically new one. Comet C/2025 A6 provides an opportunity to measure water-driven activity in a long-period comet. The OH 18-cm emission from comets is intrinsically weak and strongly dependent on solar pumping conditions, so detecting it requires high-sensitivity single-dish observations. Between January 3 and November 11, 2025, it was observable with FAST, the largest single-dish radio telescope in the world. FAST’s enormous collecting area is particularly well suited for this purpose and enables the detection of OH emission from comets. Observations of C/2025 A6 therefore help expand the currently sparse dataset of OH 18-cm measurements and provide an important benchmark for studies of cometary water production rates. In addition, a larger aperture results in a smaller beam size, providing an opportunity to measure OH line intensities at different positions within the coma. This capability provides a useful complement to observations with smaller telescopes, whose beams often encompass the entire coma and therefore measure only the beam-averaged emission. The FAST has been used for comet related studies before (e.g.,

Chen et al. 2024) with the L-band to search for the molecular spectral lines.

In this work, we present observations of the comet C/2025 A6 with FAST. Section 2 describes the observations. The data processing is mentioned in the Section 3. In Section 4, we discuss the changes of OH line profiles and production rate. The conclusion is presented in Section 5.

Table 1 OH 18-cm hyperfine transitions.

Transitions	Common designation	Frequency (MHz)
$^2\Pi_{3/2} (F = 1 - 2)$	OH 1612 MHz	1612.2309
$^2\Pi_{3/2} (F = 1 - 1)$	OH 1665 MHz	1665.4018
$^2\Pi_{3/2} (F = 2 - 2)$	OH 1667 MHz	1667.3590
$^2\Pi_{3/2} (F = 2 - 1)$	OH 1720 MHz	1720.5299

2 OBSERVATIONS

The observations of C/2025 A6 were performed with FAST (Nan et al. 2011) on October 23, 26 and from November 3 to 8 in 2025. The details can be found in Table 2. It is worth noting that the C/2025 A6 moved very quickly, all observations were conducted in the user-defined mode.

In order to observe the OH 18-cm lines at ~ 1700 MHz, the ultra-wideband (UWB) receiver (Zhang et al. 2023) covering 0.5–3.3 GHz was used. This testing receiver is not cooled and with a system temperature between 89 to 130 K. At the spectral frequency (~ 1660 MHz), the beam size is around $2.5'$. An optical image of the comet, taken with the 70-cm UCASST telescope, showing that a significant fraction of the coma is covered (Figure 1). Previous tests have shown excellent agreement between the OH flux densities and velocities measured with the FAST UWB receiver and those obtained with the Arecibo 300 m telescope (Zhang et al. 2023).

The data from the UWB receiver were separated into four sub-bands, being 0–1100, 800–1900, 1600–2700 and 2400–3500 MHz, respectively. There are 1,048,576 channels in every sub-band, corresponding to a channel width of 1049 Hz. For OH 18-cm lines, the velocity resolution is approximately 0.19 km s^{-1} . The four polarizations were recorded with an integration time of 1 s. The noise calibration signal was injected with noise diodes for 1 second and stopped for 9 seconds in every 10 seconds during the observation. The noise temperatures of the calibration signal injected to the two polarization channels are 16 and 18 K, respectively.

¹ <https://ssd.jpl.nasa.gov/horizons/>

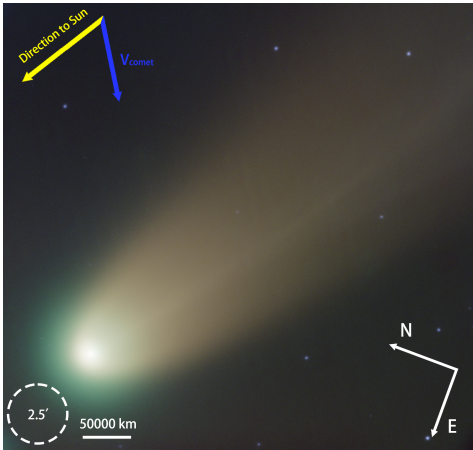


Fig. 1 Optical image of comet C/2025 A6 obtained on 2025 October 21 (18:35–18:50, UTC+8) with the 70-cm UCASST telescope. The image combines 5-min exposures in each of the R , V , and B filters and shows a coma with an apparent diameter of ~ 8 – 10 arcmin. The telescope is equipped with a 2048×2048 detector with a pixel size of $13.5 \mu\text{m}$, providing a field of view of about $20.8' \times 20.8'$. The direction towards the Sun and the comet’s heliocentric velocity are indicated with arrows.

For fast-moving targets such as the comet, we tracked the comet along its predicted trajectory by updating the telescope pointing every 0.1 s during the observation. In order to find any possible background sources which may affect the comet’s spectra, positions around the comet were also observed in the observation on November 6th. These positions were at least $3'$ off the comet nuclei.

3 DATA REDUCTION

Due to the limitation of sideband suppression of the UWB, only the bands 500–950, 950–1750, 1750–2550, and 2550–3300 MHz were used (Zhang et al. 2023). We searched for the CH lines in the 500–950 MHz sub-band. However, as the UWB receiver is still under commissioning, this band is significantly affected by radio frequency interference (RFI), and no CH line was detected. The OH 18-cm lines are located within the 800–1900 MHz sub-band, which is comparatively less affected by RFI. Thus, only the spectra in this frequency range were used in our study. For each cycle, the temperature corresponding to the measured power is determined by differencing the spectral line data acquired with open and closed noise diode, followed by calibrating the resulting power values of all spectral lines into temperature. The calibrated spectral data are processed using the astronomical data

processing software GILDAS/CLASS². For all observations, a second-order polynomial baseline was fitted and subtracted over a velocity span of 60 km s^{-1} around the line, excluding the channels containing line emission, absorption features, or identifiable RFI.

The spectra were then smoothed with a two-channel boxcar window, yielding a velocity resolution of about 0.38 km s^{-1} . All spectra were combined with a sigma-weighted averaging.

We performed Gaussian fitting on all spectra with clear detections to obtain the integrated intensity, line-center velocity, FWHM, and peak amplitude of the OH 18-cm lines. We also applied a trapezoidal fitting procedure to the 1667 MHz spectra of the four observations with detections October 23, 26 and November 4, 5 in order to derive the half-width of the trapezoidal base. The derived parameters are summarized in Table 3.

For whom may interested in the conversion from the brightness temperature to the flux with FAST data, the details can be found in appendix A.

4 RESULTS AND DISCUSSION

During four observing epochs on October 23, 26 and November 4, 5, either emission or absorption of the 1667 MHz line was detected.

4.1 Change of OH 18-cm Lines from Emission to Absorption

In our observations, the OH 18-cm lines exhibit a clear evolution from emission to absorption. During the first two observing epochs, the OH lines are detected in emission in both the 1665 and 1667 MHz transitions, with corresponding line-center velocities of 13.4 km s^{-1} and 28.8 km s^{-1} , respectively. In subsequent observations, the lines appear in absorption in both main lines, with a stronger signal at 1667 MHz. The corresponding line-center velocities are 53.5 km s^{-1} , 56.4 km s^{-1} , and 57.0 km s^{-1} on November 3 to 5, respectively. The fitted line-center velocities are consistent with the expected topocentric radial velocities derived from JPL horizons system at each observing epoch, confirming the cometary origin of the detected signals. No distinct OH signal is detected during the observations from November 6 to 8 within the expected velocity range.

The observed transition of the OH 18-cm lines from emission to absorption indicates a change in the excitation conditions of the OH ground-state Λ -doublet population. In the cometary coma, these level

² <https://www.iram.fr/IRAMFR/GILDAS/>

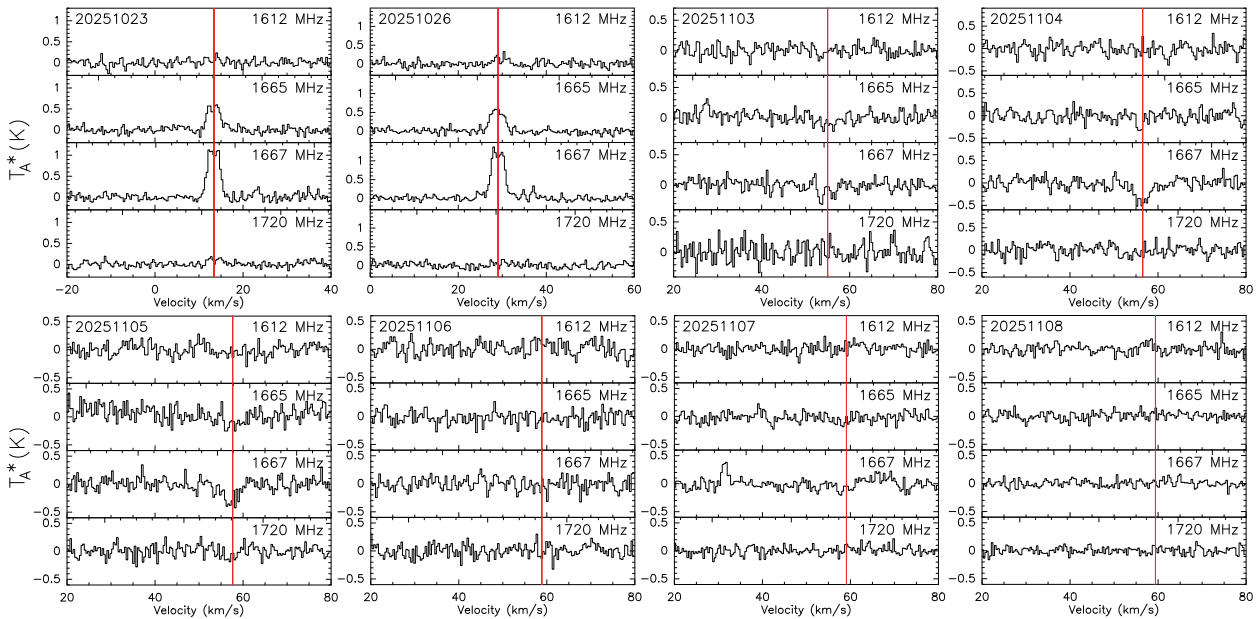


Fig. 2 The OH 18-cm lines obtained on the individual observing dates. All spectra were processed with a two-channel boxcar smoothing, yielding a final velocity resolution of 0.38 km s^{-1} . The OH main lines show emission on October 23 and 26, and transition to absorption starting on November 3. No significant OH signal was detected during November 6 to 8. The red vertical line indicates the comet's topocentric radial velocity, as computed from the JPL Horizons system.

results in a very weak OH signal. Another possibility is that the geocentric distance increased by a factor of 1.7, from 0.60 AU on October 23 to 1.01 AU on November 8, as the comet was moving away from the Earth. Consequently, the OH intensity may have fallen below the sensitivity limit of the telescope, leading to a non-detection.

4.2 Water Expansion Velocities from OH Lines

The OH coma is commonly described using a spherically symmetric, steady-state, and isotropic outflow model, in which OH is treated as a secondary product of H_2O photodissociation. The velocity of OH molecules is determined by the expansion velocity of the parent gas, v_p , combined with an additional ejection velocity due to photodissociation, v_d (Bockelée-Morvan & Gerard 1984; Crovisier et al. 2002). The OH 18-cm lines profiles can be well reproduced by trapezoidal fitting, where the width of the lower base corresponds to $2(v_d + v_p)$. This trapezoidal profile model has been widely applied in cometary OH line studies (Drozdovskaya et al. 2023; Li et al. 2025; Sakai et al. 2025). Although OH line profiles always display asymmetries due to anisotropic outgassing toward the Sun or Earth (Li et al. 2025), such effects have only a limited impact on the determination of the lower-base width (Bockelée-Morvan & Gerard 1984). In this

work, we adopt a value of $v_d = 0.95 \text{ km s}^{-1}$ to represent the ejection velocity of OH radicals following the photodissociation of H_2O , based on the analyses presented in (Crovisier et al. 2002; Tseng et al. 2007). This value is consistent with the typical OH ejection speeds reported in previous cometary studies (Crovisier 1989; Bockelée-Morvan et al. 1990). The resulting values of $v_d + v_p$ derived from the symmetric trapezoidal fits are listed in Table 3.

4.3 The estimate of OH production rate

The OH production rate can be estimated by (Schloerb & Gerard 1985; Bockelée-Morvan et al. 1990):

$$f\Gamma = 2.33 \times 10^{34} \frac{\Delta^2 S}{iT_{\text{bg}}} \quad (2)$$

and

$$Q_{\text{OH}} = \frac{\Gamma}{\tau_{\text{OH}}}, \quad (3)$$

where Γ is the total number of OH radicals in the coma, S is the integrated intensity of the 1667 MHz line in units of Jy km s^{-1} , i is the inversion of the ground state, and Δ is the geocentric distance of the comet in AU. T_{bg} denotes the background temperature in the unit of K, τ_{OH} is the OH lifetime, and f is correction factor. For τ_{OH} , it can be expressed

as: $\tau_{\text{OH}} = \tau_{\text{OH}(1\text{AU})} \times r_h^2$ (Wang et al. 2017; Sakai et al. 2025), and $\tau_{\text{OH}(1\text{AU})}$ was estimated as 1.1×10^5 s from Bockelée-Morvan et al. (1990), where the r_h is the heliocentric distance of the comet. Following the method of Crovisier et al. (2002), we estimated T_{bg} using the 1420 MHz brightness temperature distribution. The 1420 MHz map was obtained from the NASA/LAMBDA³ Stockert–Villa-Elisa all-sky survey (Reich 1982; Reich & Reich 1986; Testori et al. 2001), and the corresponding background temperature T_{bg} is listed in Table 3. The inversion of ground state at the corresponding coma velocity is obtained from (Schleicher & A’Hearn 1988) and listed in Table 3.

Since the FAST beam is considerably smaller than the characteristic size of the OH coma, a beam-size correction is required to account for flux losses outside the beam. We therefore apply the correction factor f to convert the observed number of OH radicals within the beam to the total OH population in the coma. It can be expressed as:

$$f = \frac{\int_0^{+\infty} N(\rho)\omega(\rho)\rho d\rho}{\int_0^{+\infty} N(\rho)\rho d\rho} \quad (4)$$

where $N(\rho)$ is the OH column density distribution derived from Haser model. The expansion velocity v_p is derived from the trapezoidal fits, and the photodissociation lifetime of H_2O at 1 AU is adopted as 4.6×10^4 s (Huebner et al. 1992), also scaling as r_h^2 . The beam weighting function $\omega(\rho)$ is assumed to be Gaussian, with a FWHM of 2.5 arcmin.

For small heliocentric distances, the inversion of the OH ground state is quenched by the collision of ions and electrons. Neglecting the contribution of the quenched region will lead to an underestimate of the OH production rate. However, owing to the small FAST beam, which is comparable in size to the quenching region, the iterative quenching correction fails to converge for our observational configuration. Details are provided in Appendix B.

When only the beam correction is applied, the derived Q_{OH} values serve as lower limits, with value of $(1.0 \pm 0.1) \times 10^{29}$, $(1.2 \pm 0.1) \times 10^{29}$, $(1.4 \pm 0.3) \times 10^{29}$, and $(1.5 \pm 0.4) \times 10^{29} \text{ s}^{-1}$ for October 23, 26 and November 4, 5, respectively. The Q_{OH} production rate basically increases as the heliocentric distance decreases. The water production rate of comet can be approximated as $Q_{\text{H}_2\text{O}} = 1.1 Q_{\text{OH}}$ (e.g., Sakai et al. 2025; Li et al. 2025).

³ <https://lambda.gsfc.nasa.gov/product>

5 CONCLUSIONS

We present FAST observations of the OH 18-cm lines in comet C/2025 A6 obtained between October 23 and November 8. Our main results and conclusions can be summarized as follows:

1. We confirm that the detected OH 18-cm signals originate from the cometary coma. This conclusion is supported by (i) the agreement between the fitted line-center velocities and topocentric radial velocity of the comet, and (ii) the On–Off observations, in which no emission is detected at the offset positions along the comet’s trajectory. We detected the OH main lines in emission on October 23, 26 and in absorption on November 3 to 5. The observed emission-to-absorption transition is consistent with the dependence of the OH inversion parameter on heliocentric radial velocity through the Swings effect, which can drive the inversion parameter across zero.
2. We fitted the detected OH line profiles with a trapezoidal model and derived the corresponding parent expansion velocities. The results show that the expansion velocity increases as the heliocentric distance decreases, in agreement with expectations for solar-driven cometary outgassing.
3. Using the measured 1667 MHz line intensities and applying beam-size and quenching corrections, we estimate a plausible range of OH production rates and derive lower limits on Q_{OH} . The results show a general increase with decreasing heliocentric distance.

Future observations sampling multiple positions across the coma, or coordinated observations using beams of different sizes, will mitigate systematic uncertainties associated with collisional quenching and provide more robust constraints on Q_{OH} .

Acknowledgements We would like to thank the anonymous reviewers for their constructive suggestions, which have greatly improved the quality of this paper. This work is supported by the National Key R & D Program of China No. 2025SKA0140100, No. 2022YFC2205202, No. 2020SKA0120100, No. 2025SKA0140101 and the National Natural Science Foundation of China (NSFC, Grant Nos. 11703047, 12373032, 12003047, 11773041, U2031119, 12173052, and 12173053). Both Lei Qian and Zhichen Pan were supported by the Youth Innovation Promotion Association of CAS (id. 2018075, Y2022027, and 2023064) and the CAS “Light of West China” Program. Hongfei Liu has been supported by the National Natural Science Foundation of China (NSFC) under No.12273072. Liyun Zhang has been supported by the Science and Technology Program

so that OH radicals within this region do not contribute to the observable 18-cm signal (Despois et al. 1981), and the factor f can be written as:

$$f = \frac{\int_0^{+\infty} N'(\rho)\omega(\rho)\rho d\rho}{\int_0^{+\infty} N(\rho)\rho d\rho} \quad (\text{B.1})$$

Where the $N'(\rho)$ is the column density distribution after subtracting the sphere with radius r_q . The quenching radius r_q can be expressed as $r_q = r_q^* r_h \sqrt{Q_{\text{OH}}/10^{29}}$ (e.g., Li et al. 2025). Adopting $r_q^* = 47,000$ following Li et al. (2025) results in unstable convergence. We therefore adopt a reduced value of r_q^* to ensure convergence. With this treatment, the derived Q_{OH} values for October 23, 26 and November 4, 5 are $(2.4 \pm 0.3) \times 10^{29}$, $(2.8 \pm 0.3) \times 10^{29}$, $(3.6 \pm 0.5) \times 10^{29}$, and $(3.9 \pm 1.0) \times 10^{29} \text{ s}^{-1}$, respectively.